Solid-State Fluorescence

Deutsche Ausgabe: DOI: 10.1002/ange.201602502
Internationale Ausgabe: DOI: 10.1002/anie.201602502

Engineering Stacks of V-Shaped Polyaromatic Compounds with Alkyl Chains for Enhanced Emission in the Solid State

*Shoya Sekiguchi, Kei Kondo, Yoshihisa Sei, Munetaka Akita, and Michito Yoshizawa**

Abstract: *A V-shaped bisanthracene derivative with three butyl groups formed two types of emissive solids that display bluish green and blue fluorescence ($\Phi_F = 72$ and 32 %, respectively), depending on the preparation conditions. The crystal and powder X-ray analyses reveal that the highly emissive solid adopts a head-to-head arrangement with discrete stacks of the anthracene moieties, whereas the moderately emissive solid adopts a head-to-tail arrangement without the stacks. The obtained molecular arrangements are transformed by thermal stimuli accompanying the change in fluorescence. Furthermore, large enhancements of dye emissions (12–45-fold) through highly efficient host–guest energy transfer were achieved in the solid state by adding minute amounts of various fluorescent dyes (e.g. rubrene and Nile red) to the V-shaped compound.*

Polyaromatic compounds with peripheral substituents often form well-ordered columnar stacks in the solid state (Figure 1 a).[1] However, the emissive ability of the polyaromatic moieties found in dilute solutions is apt to be lost or weakened in such infinite structures owing to nonradiative decay of the excited states through extensive aromatic–aromatic interactions. Full encirclement of polyaromatic compounds by molecular capsules[2,3] or bulky substituents[4–6] can prevent infinite stacking of the fluorophores (Figure 1 b) so that most of them show simple emissions from the monomeric species. In contrast, dimeric stacks of polyaromatic molecules have received considerable attention, because their structures sometimes exhibit intriguing fluorescence behavior derived from the formation of excimers.[7] However, there is no general and rational approach to prepare highly fluorescent dimeric stacks of polyaromatic compounds through noncovalent interactions.[8] To exploit a new class of polyaromatic solids with a greater emissive ability, we designed a V-shaped polyaromatic compound bearing bulky substituents on the convex side to engineer 1) the dimeric stack of the bent polyaromatic frameworks (Figure 1 c) and 2) the layered arrays of the polyaromatic dimers through intermolecular interactions between the substituents. Here we report the unusual emission behavior of V-shaped bisanthracene derivative **1** with three butyl groups (Figure 1 d) in the solid state.

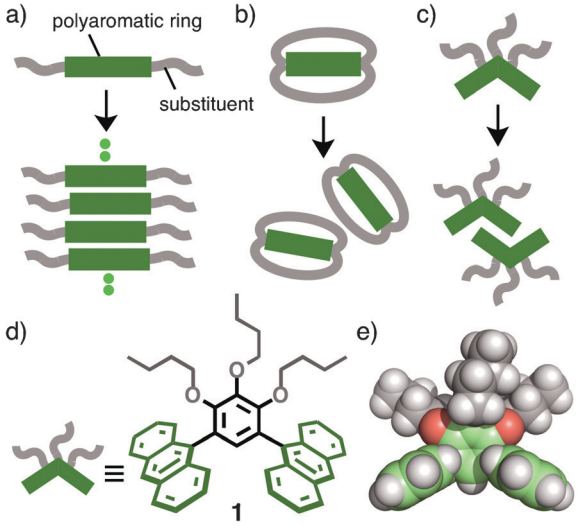

Figure 1. Schematic representations of a) the infinite stack and b) the isolation of planar polyaromatic compounds with substituents, and c) the discrete stack of bent polyaromatic compounds with substituents on the convex side. d) V-Shaped bisanthracene derivative **1** designed herein and e) the optimized structure (DFT calculation, B3LYP/6-31G* level).

The V-shaped compound forms two different types of solids depending on the preparation conditions. The solid with a head-to-head arrangement (Figure 1 c) shows strong bluish green fluorescence ($\Phi_F = 72\,\%$) as a consequence of finite stacks of the anthracene moieties. In contrast, the other solid with a head-to-tail arrangement shows moderate blue fluorescence ($\Phi_F = 32\,\%$). The molecular arrangement and emissive states can be changed by thermal stimuli. In addition, the solid-state emission properties of various fluorescent dyes (e.g. rubrene and Nile red) are greatly enhanced (12–45-fold) by mixing them with the bisanthracene derivative upon single irradiation with UV light (e.g. $\lambda = 368$ nm), because of highly efficient energy transfer from the anthracene moieties to the dyes.

In this study, we initially focused on a V-shaped polyaromatic framework[9] composed of two anthracene panels linked by a *meta*-phenylene spacer with hydroxy groups because of its rigid and bent structure as well as appropriately stable and fluorescent character.[10] We expected that the functionalization of the bent framework with three alkyl chains on the convex side could generate highly emissive solids through engineered aromatic–aromatic (i.e. π-stacking) and alkyl–alkyl (i.e. van der Waals) interactions. The *n*-butyl group was employed as a suitable substituent to fully cover the *exo*-polyaromatic surface of the V-shaped framework

[*] S. Sekiguchi, Dr. K. Kondo, Dr. Y. Sei, Prof. Dr. M. Akita, Dr. M. Yoshizawa
Chemical Resources Laboratory
Tokyo Institute of Technology
4259 Nagatsuta, Midori-ku, Yokohama 226-8503 (Japan)
E-mail: yoshizawa.m.ac@m.titech.ac.jp

Supporting information for this article can be found under: http://dx.doi.org/10.1002/anie.201602502.

(Figure 1e), thereby enabling compound **1** to form a dimeric stack between the *endo*-polyaromatic surfaces in the solid state.

V-Shaped compound **1** was synthesized from 1,2,3-trimethoxybenzene in 60% overall yield (4 steps) and its structure was confirmed by NMR spectroscopy, MS, and elemental analyses (Figures S1–9).[11] A solution of **1** in CH_2Cl_2 showed electronic absorption bands at $\lambda = 310$–410 nm (Figure 2a)

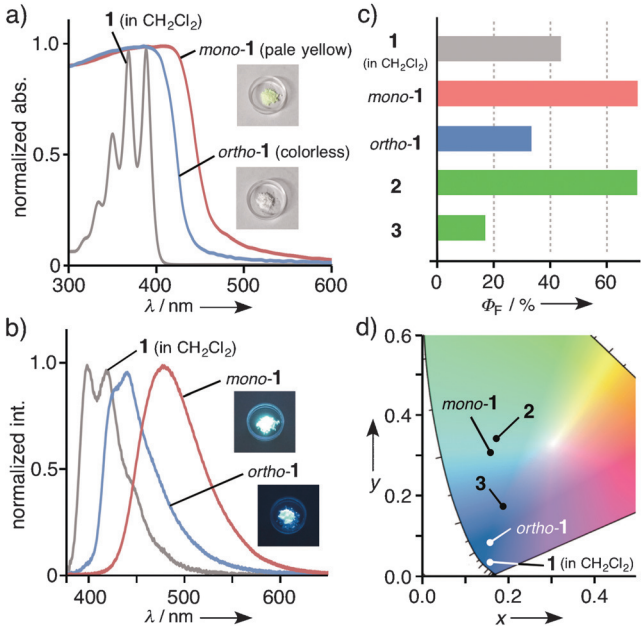

Figure 2. a) UV/Vis and b) fluorescence spectra (RT, $\lambda_{ex} = 368$ nm) of solids *mono*-**1** and *ortho*-**1**, and a solution of **1** in CH_2Cl_2 (10 μM). c) Fluorescence quantum yields (Φ_F) and d) CIE coordinate diagram of solids *mono*-**1**, *ortho*-**1**, **2**, and **3**, and a solution of **1** in CH_2Cl_2.

assigned to typical π-π* transitions of the anthracene moieties and emission bands at $\lambda = 380$–530 nm (Figure 2b; $\lambda_{ex} = 368$ nm, $\Phi_F = 43\%$) originating from the monomeric species. Interestingly, we obtained two types of fluorescent solids from **1** that display different spectroscopic properties.[11] Evaporation of a solution of **1** in CH_2Cl_2 or $CHCl_3$ gave rise to a pale yellow solid (*mono*-**1**). On the other hand, a colorless solid (*ortho*-**1**) was obtained by the same procedure from a solution of **1** in CH_3CN or CH_3OH. The solid-state UV/Vis spectra disclosed that *mono*-**1** shows a broad absorption band around 430 nm, which is red-shifted ($\Delta\lambda_{max} = 56$ nm) compared with that of *ortho*-**1** (Figure 2a). Solid *mono*-**1** emitted strong bluish green fluorescence with an emission band at $\lambda_{max} = 481$ nm and with a high quantum yield ($\Phi_F = 72\%$) upon irradiation at $\lambda = 368$ nm. Notably, the fluorescence quantum yield is 1.7-times higher than that of **1** in CH_2Cl_2 solution (Figure 2b,c).[12] The emission band of solid *mono*-**1** was significantly shifted ($\Delta\lambda \approx 80$ nm) compared with that of the solution, most probably because of effective aromatic–aromatic interactions between the anthracene panels. In contrast, solid *ortho*-**1** emitted blue fluorescence ($\lambda_{max} = 442$ nm) with a moderate quantum yield ($\Phi_F = 32\%$) that is 2.3-times lower than that of *mono*-**1** (Figure 2b,c). The difference in the total emission colors of solids *mono*-**1** and *ortho*-**1** was quantified by a CIE chromaticity diagram (Figure 2d).[13] The huge differences between *mono*-**1** and *ortho*-**1** in terms of the fluorescence wavelength ($\Delta\lambda = 56$ nm) and intensity (2.3-fold) originate from the solid-state molecular ordering, as revealed by crystal and powder X-ray analyses.

The detailed molecular arrangements of *mono*-**1** and *ortho*-**1** in the solid state were elucidated by X-ray crystallographic analysis. Pale yellow crystals of *mono*-**1** and colorless crystals of *ortho*-**1** were grown by slow concentration of solutions of **1** in CH_2Cl_2/CH_3CN (> 10 mM for *mono*-**1** and < 1.0 mM for *ortho*-**1**) at room temperature. In the crystal structure (monoclinic space group) of highly emissive *mono*-**1**, V-shaped compound **1** forms a head-to-head dimer, which is arranged in a multiply layered structure composed of an alternating polyaromatic layer with a thickness of about 10 Å and an aliphatic layer with a thickness of about 5 Å (Figure 3a,b and Table S2a). Within the polyaromatic layers, one

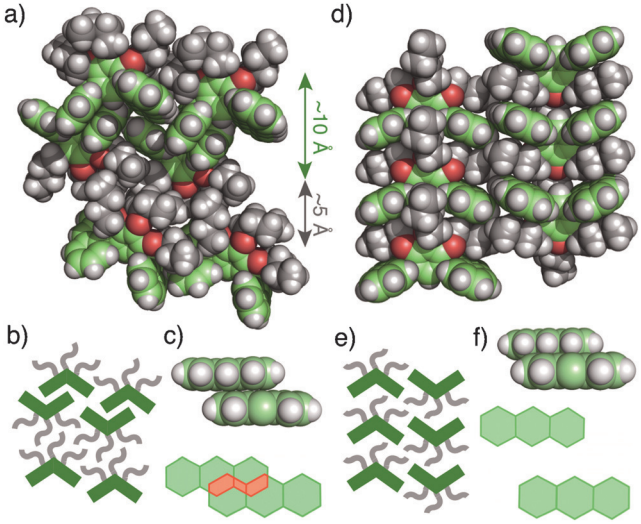

Figure 3. X-ray crystal structures and molecular arrangements of a) *mono*-**1** (monoclinic space group) and d) *ortho*-**1** (orthorhombic space group). Schematic representations of b) the head-to-head arrangement of *mono*-**1** and e) the head-to-tail arrangement of *ortho*-**1**. The stacking patterns of the closely located two anthracene panels of c) *mono*-**1** and f) *ortho*-**1** (side and top views).

of the two anthracene rings of **1** is partially π-stacked with that of another molecule of **1** with an interplanar distance of 3.4 Å and with an overlapping area of 27% (Figure 3c). Intermolecular CH–π interactions between the anthracene rings are also found within the layers. The aliphatic layers show that the alkyl chains are closely aggregated with each other through van der Waals interactions without solvent molecules. In sharp contrast, the crystal structure (orthorhombic space group) of moderately emissive *ortho*-**1** contains one-dimensional columnar stacks with a head-to-tail arrangement that are arranged in an antiparallel fashion (Figure 3d,e and Table S2b). Each of the anthracene rings is separated by the alkyl chains, so that intermolecular π-stacking interactions

between the anthracene moieties were completely prevented (Figure 3 f).

In powder X-ray diffraction analysis, both solids *mono*-**1** and *ortho*-**1** displayed crystalline powder patterns, which resembled those obtained from the corresponding crystals, respectively (Figures S24 and S25). Therefore, the molecular arrangements of the bent polyaromatic framework greatly govern the fluorescence features in the solid state. The high fluorescence efficiency ($\Phi_F \approx 70\,\%$) of solid *mono*-**1** likely stems from the increase in the structural rigidity of the anthracene fluorophores through discrete, head-to-head π-stacking interactions and CH–π interactions, as supported by excited-state dynamics studies.[14] The fluorescence lifetime (τ_s) of solid *mono*-**1** was estimated to be 92.2 ns, whereas that of *ortho*-**1** is very short (5.3 ns). Solid *ortho*-**1** shows a monomer-like emission with moderate efficiency ($\Phi_F \approx 30\,\%$), similar to the emission properties of **1** in CH_2Cl_2, as a consequence of the absence of π-stacking interactions between the anthracene moieties.

The butyl groups on the V-shaped framework of **1** are essential for the formation of the two types of solids with the different fluorescence properties. We next sought to clarify the effect of the substituents on the bent polyaromatic compound by synthesizing analogues of **1** having longer and shorter alkyl chains; this was achieved in one step from the precursor of **1**.[11] V-Shaped bisanthracene derivative **2** with the longer *n*-hexyl groups afforded a fluorescent solid with highly emissive properties ($\Phi_F = 73\,\%$) similar to those of solid *mono*-**1** (Figure 2 c,d and Figure S22). This result most probably arises from the formation of a head-to-head arrangement of **2** through enhanced, intermolecular alkyl–alkyl interactions. On the other hand, bisanthracene derivative **3** with the shorter ethyl groups gave a moderately fluorescent solid ($\Phi_F = 17\,\%$). The emission wavelengths and quantum yields of solids **2** and **3** are insensitive to the preparation conditions, in contrast to solid **1**.

It should be noted that the solid-state emission properties of **1** can be markedly changed by thermal stimuli. The fluorescence maximum of solid *ortho*-**1** moves from $\lambda = 442$ to $\lambda = 471$ nm upon heating it at 110 °C for 15 min (Figure 4 a). The emission band of the resultant solid (*mono*-**1**′) is similar to that of solid *mono*-**1** (Figure 2 b). Further heating of the solid at 140 °C for 15 min resulted in it transforming into another solid (*amo*-**1**) with a fluorescence maximum at $\lambda =$ 441 nm ($\Phi_F = 12\,\%$; Figure 4 b). Differential thermal analysis (DTA) over a range of 50 to 200 °C revealed that solid *ortho*-**1** has two endothermic peaks at 108 and 138 °C (Figure 4 c), which can be assigned to a phase transition temperature and a melting temperature, respectively. Thermal gravimetric (TG) analysis of *ortho*-**1** proved that there is no decrease in the mass at temperatures below 250 °C. The observed structural deformations were further confirmed by powder X-ray diffraction analysis. The diffraction pattern of solid *ortho*-**1** (Figure 4 d)[15] changed upon heating it at 120 °C for 15 min, and the resultant diffraction pattern (Figure 4 e) is partially superimposable on that of solid *mono*-**1** obtained from the $CHCl_3$ solution (Figure S26 a).[11] Thus, we presumed that the produced solid (*mono*-**1**′) adopts a head-to-head arrangement similar to that of solid *mono*-**1**. Heating solid

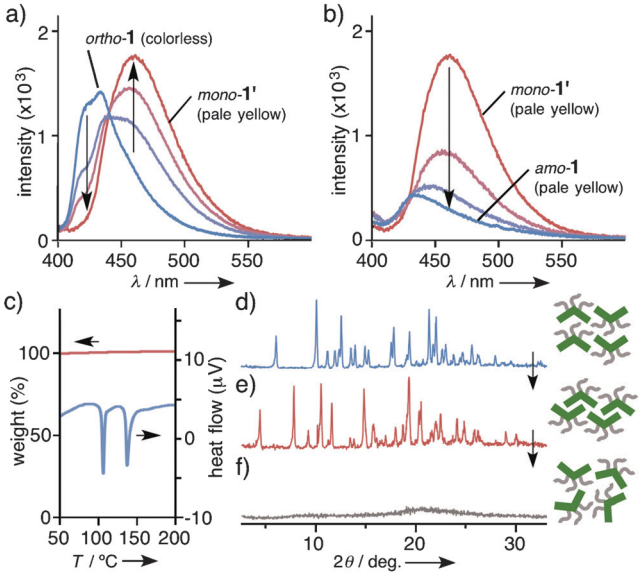

Figure 4. Solid-state fluorescence spectra (RT, $\lambda_{ex} = 368$ nm) of a) *ortho*-**1** after heating at 110 °C for 1.5, 4, and 15 min and b) *mono*-**1** after heating at 140 °C for 2, 6.5, and 15 min. c) TG-DTA curves (heating rate of 10 °C min^{-1} from 50 to 200 °C) of *ortho*-**1**. d–f) Powder X-ray diffraction patterns (RT) and schematic representations of d) solid *ortho*-**1** at RT and the resultant solids after heating at e) 120 °C and f) 150 °C for 15 min.

mono-**1**′ at 150 °C for 15 min led to amorphous solid *amo*-**1**, which exhibits considerably broadened X-ray diffraction (Figure 4 f). Notably, solids *mono*-**1** and *ortho*-**1** were readily regenerated by sequential dissolution ($CHCl_3$ and CH_3OH, respectively) and evaporation of solid *amo*-**1** (Figure S26 b). TG-DTA studies indicated that solids **2** and **3** show single endothermic peaks at 123 and 211 °C, respectively, which are assignable to the corresponding melting points (Figure S27). Therefore, the suitable balance of intermolecular alkyl–alkyl interactions enables **1** to adopt three transformable solid states that display distinct emissivities (i.e. fluorescence wavelength and quantum yield).

Finally, we examined the manipulation of the emission color of solid **1** upon addition of minute amounts of fluorescent dyes. Although common fluorescent compounds such as DCM,[16] rubrene (Rub), Nile red (NR), and tetracene (Tet) emit strong or moderate fluorescence in dilute solutions, their solids exhibit relatively weak emissions ($\Phi_F = 1$–$6\,\%$)[17] because of the notorious self-quenching effect (Figure 5 a and Figure S29). In contrast, mixed solid **1**·$(DCM)_{0.01}$, prepared by evaporation of a THF solution of **1** and DCM (0.01 equiv), displayed a strong orange emission ($\Phi_F = 52\,\%$) upon irradiation of the anthracene absorption band at $\lambda = 368$ nm (Figure 5 b,c).[18] The emission efficiency of the DCM dye was significantly enhanced (26 times) within the host solid of **1**. The solid-state fluorescence spectrum displayed a new prominent band at $\lambda_{max} = 584$ nm derived from the incorporated dye and a very weak band around $\lambda = 420$ nm derived from the anthracene moieties of **1** (Figure 5 b). These emission bands indicate highly efficient fluorescence resonance energy transfer (FRET) from **1** to DCM (96 %, as calculated from the fluorescence quenching data) in the solid

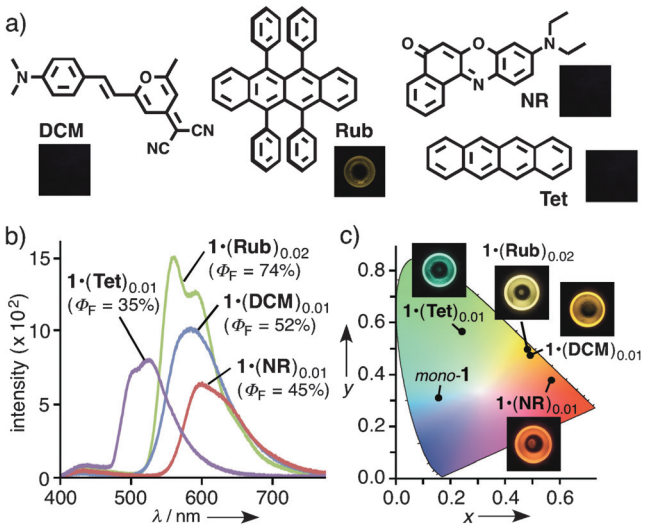

Figure 5. a) Fluorescent dyes DCM, rubrene (Rub), Nile red (NR), and tetracene (Tet) studied herein with photographs of the solids (RT, $\lambda_{ex}=365$ nm). b) Fluorescence spectra (RT, $\lambda_{ex}=368$ nm) of mixed solids **1**·$(DCM)_{0.01}$, **1**·$(Rub)_{0.02}$, **1**·$(NR)_{0.01}$, and **1**·$(Tet)_{0.01}$ and c) their CIE coordinate diagram ($\lambda_{ex}=368$ nm) with photographs ($\lambda_{ex}=365$ nm).

state.[6,19–21] Powder X-ray diffraction analysis of **1**·$(DCM)_{0.01}$ showed no crystalline peaks, thus indicating the formation of an amorphous solid (Figure S33b), which might prompt the strong fluorescence emission from the guest dye but not from the host. Furthermore, mixed solids **1**·$(Rub)_{0.02}$, **1**·$(NR)_{0.01}$, and **1**·$(Tet)_{0.01}$ emitted strong orange ($\Phi_F=74\%$), red ($\Phi_F=45\%$), and green fluorescence ($\Phi_F=35\%$), respectively, even upon irradiation with light of the same wavelength ($\lambda_{ex}=368$ nm; Figure 5b,c). The solid-state emission quantum yield of **1**·$(NR)_{0.01}$ is 45-fold higher than that of NR under the same conditions, and the FRET efficiency of the mixed solid is more than 90%. We emphasize herein that, upon single excitation with UV light, polyaromatic solids with various emission colors and relatively high emission intensities could be obtained by simple mixing **1** with a tiny amount (1–2%) of readily available fluorescence dyes.

In summary, we have developed novel polyaromatic compounds with unique emissive properties in the solid state. To avoid typical infinite stacks of planar polyaromatic moieties, we designed a V-shaped bisanthracene derivative possessing three butyl chains on the convex side. The bent polyaromatic compounds afforded two types of emissive solids, which display highly bluish-green ($\Phi_F\approx70\%$) and moderate blue fluorescence ($\Phi_F\approx30\%$) and are transformable by thermal stimuli. The crystal and powder X-ray analyses revealed that the highly emissive solid adopts a head-to-head arrangement with isolated, dimeric stacks of the anthracene fluorophores through the assistance of intermolecular aromatic–aromatic and alkyl–alkyl interactions. Thus, elongation of the alkyl groups on the bent polyaromatic framework resulted in the formation of a highly fluorescent solid ($\Phi_F=73\%$) whose emission is insensitive to the preparation conditions. In addition, we revealed that the V-shaped polyaromatic compound acts as a host material to enhance the solid-state emissivity of various fluorescent dyes (up to 45-times) through highly efficient host–guest energy transfer upon incorporation of the dyes into the solid. The present results show a new strategy to engineer the molecular alignment and interactions of polyaromatic compounds in the solid state for the development of novel photofunctional materials with superior emissive properties.

Acknowledgements

This work was supported by the Japanese Ministry of Education, Culture, Sports, Science, and Technology (MEXT) through a Grants-in-Aid for Scientific Research on Innovative Areas "Soft Molecular Systems" and by "Support for Tokyotech Advanced Researchers (STAR)". K.K. thanks the JSPS for a Research Fellowship for Young Scientists.

Keywords: anthracene · dyes/pigments · π-stacking · host–guest systems · solid-state fluorescence

How to cite: *Angew. Chem. Int. Ed.* **2016**, *55*, 6906–6910
Angew. Chem. **2016**, *128*, 7020–7024

[1] a) S. Kumar, *Chem. Soc. Rev.* **2006**, *35*, 83–109; b) S. Sergeyev, W. Pisulab, Y. H. Geerts, *Chem. Soc. Rev.* **2007**, *36*, 1902–1929.
[2] Encapsulation by organic capsules: a) S. J. Dalgarno, S. A. Tucker, D. B. Bassil, J. L. Atwood, *Science* **2005**, *309*, 2037–2039; b) L. S. Kaanumalle, C. L. D. Gibb, B. C. Gibb, V. Ramamurthy, *J. Am. Chem. Soc.* **2005**, *127*, 3674–3675; c) N. Nishimura, K. Kobayashi, *J. Org. Chem.* **2010**, *75*, 6079–6085.
[3] Encapsulation by coordination capsules: a) K. Ono, J. K. Klosterman, M. Yoshizawa, K. Sekiguchi, T. Tahara, M. Fujita, *J. Am. Chem. Soc.* **2009**, *131*, 12526–12527; b) P. P. Neelakandan, A. Jiménez, J. R. Nitschke, *Chem. Sci.* **2014**, *5*, 908–915; c) M. Yamashina, M. M. Sartin, Y. Sei, M. Akita, S. Takeuchi, T. Tahara, M. Yoshizawa, *J. Am. Chem. Soc.* **2015**, *137*, 9266–9269.
[4] Fluorescence in the solid state: a) Z. Fei, N. Kocher, C. J. Mohrschladt, H. Ihmels, D. Stalke, *Angew. Chem. Int. Ed.* **2003**, *42*, 783–787; *Angew. Chem.* **2003**, *115*, 807–811; b) C.-H. Chien, C.-K. Chen, F.-M. Hsu, C.-F. Shu, P.-T. Chou, C.-H. Lai, *Adv. Funct. Mater.* **2009**, *19*, 560–566; c) B. Chen, G. Yu, X. Li, Y. Ding, C. Wang, Z. Liu, Y. Xie, *J. Mater. Chem. C* **2013**, *1*, 7409–7417; d) J. Zhang, B. Xu, J. Chen, S. Ma, Y. Dong, L. Wang, B. Li, L. Ye, W. Tian, *Adv. Mater.* **2014**, *26*, 739–745; e) S. Sasaki, K. Igawa, G. Konishi, *J. Mater. Chem. C* **2015**, *3*, 5940–5950.
[5] Exceptional strong fluorescence ($\Phi_F=>80\%$) in the solid state: a) A. Iida, S. Yamaguchi, *Chem. Commun.* **2009**, 3002–3004; b) Y. Fujiwara, R. Ozawa, D. Onuma, K. Suzuki, K. Yoza, K. Kobayashi, *J. Org. Chem.* **2013**, *78*, 2206–2212.
[6] Fluorescence in the solvent-free liquid state: a) S. S. Babu, J. Aimi, H. Ozawa, N. Shirahata, A. Saeki, S. Seki, A. Ajayaghosh, H. Möehwald, T. Nakanishi, *Angew. Chem. Int. Ed.* **2012**, *51*, 3391–3395; *Angew. Chem.* **2012**, *124*, 3447–3451; b) S. S. Babu, M. J. Hollamby, J. Aimi, H. Ozawa, A. Saeki, S. Seki, K. Kobayashi, K. Hagiwara, M. Yoshizawa, H. Möehwald, T. Nakanishi, *Nat. Commun.* **2013**, *4*, 1969.
[7] Stacks of covalently linked bisanthracene derivatives: T. Hayashi, N. Mataga, Y. Sakata, S. Misumi, M. Morita, J. Tanaka, *J. Am. Chem. Soc.* **1976**, *98*, 5910–5913.
[8] Fluorescent dimeric stacks in the solid state: a) Z. Zhang, Y. Zhang, D. Yao, H. Bi, I. Javed, Y. Fan, H. Zhang, Y. Wang, *Cryst. Growth Des.* **2009**, *9*, 5069–5076; b) Y.-X. Li, H.-B. Zhou, J.-L. Miao, G.-X. Sun, G.-B. Li, Y. Nie, C.-L. Chen, Z. Chena, X.-T.

Tao, *CrystEngComm* **2012**, *14*, 8286 – 8291; c) K. Nagarajan, S. K. Rajagopal, M. Hariharan, *CrystEngComm* **2014**, *16*, 8946 – 8949; d) S. Hisamatsu, H. Masu, M. Takahashi, K. Kishikawa, S. Kohmoto, *Cryst. Growth Des.* **2015**, *15*, 2291 – 2302.

[9] The framework acts as a building block for various hollow nanostructures (e.g. capsules, tubes, and bowls) in solutions: a) N. Kishi, Z. Li, K. Yoza, M. Akita, M. Yoshizawa, *J. Am. Chem. Soc.* **2011**, *133*, 11438 – 11441; b) K. Hagiwara, Y. Sei, M. Akita, M. Yoshizawa, *Chem. Commun.* **2012**, *48*, 7678 – 7680; c) K. Yazaki, N. Kishi, M. Akita, M. Yoshizawa, *Chem. Commun.* **2013**, *49*, 1630 – 1632; d) K. Kondo, A. Suzuki, M. Akita, M. Yoshizawa, *Angew. Chem. Int. Ed.* **2013**, *52*, 2308 – 2312; *Angew. Chem.* **2013**, *125*, 2364 – 2368; e) A. Suzuki, K. Kondo, M. Akita, M. Yoshizawa, *Angew. Chem. Int. Ed.* **2013**, *52*, 8120 – 8123; *Angew. Chem.* **2013**, *125*, 8278 – 8281; f) N. Kishi, M. Akita, M. Yoshizawa, *Angew. Chem. Int. Ed.* **2014**, *53*, 3604 – 3607; *Angew. Chem.* **2014**, *126*, 3678 – 3681; g) K. Yazaki, Y. Sei, M. Akita, M. Yoshizawa, *Nat. Commun.* **2014**, *5*, 5179.

[10] Dimerization of the anthracene moieties of **1** under irradiation with UV light was not observed in previous and the present studies.

[11] See the Supporting Information.

[12] The solid of a previously reported V-shaped bisanthracene derivative with hydrophilic groups (i.e. trimethylammonium groups) shows very weak fluorescence ($\Phi_F = < 3\,\%$), whereas its CH_3OH solution exhibits moderate fluorescence ($\Phi_F = 34\,\%$).[9d]

[13] CIE chromaticity values: solids *mono*-**1** (0.16, 0.30), *ortho*-**1** (0.16, 0.08), **2** (0.17, 0.34), and **3** (0.19, 0.17), and a solution of **1** in CH_2Cl_2 (0.16, 0.03).

[14] Single exponential decays from the singlet excited states were observed in the crystalline solids *mono*-**1** and *ortho*-**1** by time-resolved fluorescence spectroscopy (Table S1). The nonradiative decay rate constant (k_{nr}) for *mono*-**1**, calculated from the Φ_F and τ_s values, is $3.0 \times 10^6\ s^{-1}$, which is smaller than that of *ortho*-**1** ($1.3 \times 10^8\ s^{-1}$), thereby indicating that the nonradiative decay process is suppressed by the enhanced rigidity of the anthracene panels in the head-to-head arrangement.

[15] The powder X-ray diffraction peaks of solids *mono*-**1** and *ortho*-**1** were superimposable on the calculated peaks obtained from the corresponding X-ray crystal structures (Figure S25).

[16] DCM = 4-(dicyanomethylene)-2-methyl-6-(4-dimethylaminostyryl)-*4H*-pyran.

[17] Solid-state fluorescence quantum yields ($\lambda_{ex} = 368$ nm): DCM (2 %), Rub (6 %), NR (1 %), and Tet (1 %; Figure S29a).

[18] Upon irradiation of the absorption band of DCM at 500 nm, mixed solid **1**·$(DCM)_{0.01}$ showed a similar orange emission at $\lambda_{max} = 581$ nm with $\Phi_F = 54\,\%$ (Figure S32). The fluorescence lifetime (τ_s) of the mixed solid was estimated to be 3.5 ns, which is much shorter than that of *mono*-**1** (Figure S35).

[19] Host–guest FRET emissions in organic gels: a) A. Ajayaghosh, S. J. George, V. K. Praveen, *Angew. Chem. Int. Ed.* **2003**, *42*, 332 – 335; *Angew. Chem.* **2003**, *115*, 346 – 349; b) A. Ajayaghosh, C. Vijayakumar, V. K. Praveen, S. S. Babu, R. Varghese, *J. Am. Chem. Soc.* **2006**, *128*, 7174 – 7175; c) A. Ajayaghosh, V. K. Praveen, C. Vijayakumar, S. J. George, *Angew. Chem. Int. Ed.* **2007**, *46*, 6260 – 6265; *Angew. Chem.* **2007**, *119*, 6376 – 6381; d) A. Ajayaghosh, V. K. Praveen, S. Srinivasan, R. Varghese, *Adv. Mater.* **2007**, *19*, 411 – 415; e) C. Vijayakumar, V. K. Praveen, K. K. Kartha, A. Ajayaghosh, *Phys. Chem. Chem. Phys.* **2011**, *13*, 4942 – 4949; f) X. Wang, P. Duan, M. Liu, *Chem. Asian J.* **2014**, *9*, 770 – 778; g) V. K. Praveen, C. Ranjith, N. Armaroli, *Angew. Chem. Int. Ed.* **2014**, *53*, 365 – 368; *Angew. Chem.* **2014**, *126*, 373 – 376.

[20] Host–guest FRET emissions in the crystalline state: a) M. Pope, H. P. Kallmann, P. Magnante, *J. Chem. Phys.* **1963**, *38*, 2042 – 2043; b) H. P. Li, L. Duan, D. Q. Zhang, G. F. Dong, L. D. Wang, Y. Qiu, *Sci. China Ser. B* **2009**, *52*, 181 – 187.

[21] A fluorescence emission of the solid of 9,10-diphenylanthracene (DPA) is relatively weak ($\Phi_F = 23\,\%$). A mixed solid of DPA and DCM (1 %) showed two fluorescence bands ($\Phi_F = 30\,\%$) derived from both DPA and DCM under the same conditions (Figure S34).

Received: March 11, 2016
Published online: April 27, 2016

